Journal of proteome research

Article

pubs.acs.org/jpr

Metabolic Characterization of *Leishmania major* Infection in Activated and Nonactivated Macrophages.

Sabrina D. Lamour,[†] Beak-San Choi,[‡] Hector C. Keun,[†] Ingrid Müller,*[,‡] and Jasmina Saric*[,†]

[†]Biomolecular Medicine, Department of Surgery and Cancer, Faculty of Medicine, Imperial College London, Sir Alexander Fleming Building, South Kensington, London SW7 2AZ, United Kingdom

[‡]Department of Medicine, Section of Immunology, Faculty of Medicine, Imperial College London, London W2 1PG, United Kingdom

ABSTRACT: Infection with *Leishmania spp*. can lead to a range of symptoms in the affected individual, depending on underlying immune-metabolic processes. The macrophage activation state hereby plays a key role. Whereas the L-arginine pathway has been described in detail as the main biochemical process responsible for either nitric oxide mediated parasite killing (classical activation) or amplification of parasite replication (alternative activation), we were interested in a wider characterization of metabolic events *in vitro*. We therefore assessed cell growth medium, parasite extract, and intra- and extracellular metabolome of activated and nonactivated macrophages, in presence and absence of *Leishmania major*. A metabolic profiling approach was applied combining ^{1}H NMR spectroscopy with multi- and univariate data treatment. Metabolic changes were observed along both conditional axes, that is, infection state and macrophage activation, whereby significantly higher levels of potential parasite end products were found in parasite exposed samples including succinate, acetate, and alanine, compared to uninfected macrophages. The different macrophage activation states were mainly discriminated by varying glucose consumption. The presented profiling approach allowed us to obtain a metabolic snapshot of the individual biological compartments in the assessed macrophage culture experiments and represents a valuable read out system for further multiple compartment *in vitro* studies.

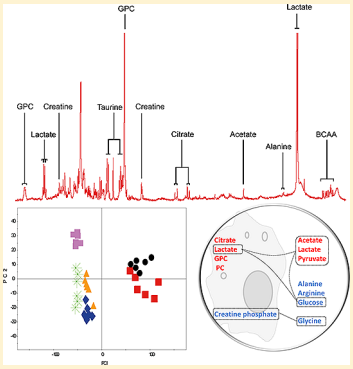

KEYWORDS: *metabolic profiling, metabolomics, Leishmania major, macrophage activation, ^{1}H NMR spectroscopy, multivariate data analysis*

INTRODUCTION

The genus *Leishmania spp*. describes a cluster of protozoan parasites that cause a variety of related disease patterns with main relevance in low income countries of the tropics and subtropics and around the Mediterranean basin. More recent figures indicate 50000 deaths and 2 million new infections each year[1] mainly due to suboptimal disease management including diagnosis, prognosis, and treatment.

Infective *Leishmania* promastigotes are injected by the sandfly vector (*Lutzomya spp*. and *Phlebotomus spp*.) into the skin of the mammalian host and are taken up by mononuclear phagocytic cells, especially macrophages and neutrophils. The main place of residence and proliferation of *Leishmania* (*L*.) *spp*. is the macrophage phagolysosome[2] where the physico-chemical conditions, in particular the high temperature and low pH initiate transformation from flagellated promastigote to immobile amastigote stage which proliferates via binary fission. Completion of the life cycle is granted when parasite-containing macrophages are taken up by the vector during a blood meal and the amastigotes are transformed back into promastigotes in the midgut. The promastigotes differentiate into infective metacyclics and migrate to the proboscis to be injected into the mammalian host.[3]

Disease development is strongly linked to parasite species and immune status of the host. While *L. aethiopica, L. major* and *L. tropica* are dermotropic species for which proliferation is usually restricted to the primary site of inoculation, the dermo-mucotropic (*L. braziliensis, L. panamanensis*) and viscerotropic species (*L. donovani, L. infantum*) can spread to mucosa and internal organs, respectively.[4,5]

Although the tropism of the various *Leishmania* strains is a major contributor to disease outcome, the state of the host's immune system is also influential and can, especially in the immune-suppressed individual, induce a spread of parasites to unusual locations such as the gastro-intestinal or respiratory tract during the visceral form of disease.[6]

Early observations on murine *L. major* infection models showed a varying disease outcome in different mouse strains, whereby the self-healing course in C57BL/6 and the progressive infection in BALB/c mice have probably been most characterized and scientifically exploited.[7−10] Due to the clear distinctive course of pathology depending on the rodent model chosen, *L. major* has been an important tool in defining the mechanisms of an effective immune response to intra-

Received: April 5, 2012
Published: June 22, 2012

dx.doi.org/10.1021/pr3003358 | *J. Proteome Res.* 2012, 11, 4211−4222

cellular pathogens. The system has substantially contributed to basic immunological understanding in infection by confirming the general mechanistic trends of T helper cell subpopulations[11] and their specific role in micro- and macro-parasite defense. The original classification into two dichotomous T helper (Th) cell populations had to be reshaped in the past decade due to other emerging Th subsets including Th17 and T regulatory cells[12] and the substantiation of the emerging concept of T cell plasticity.[13,14] However, the original simplification can still offer a gross mechanistic guidance on the cellular as well as on the metabolic level.

The L-arginine pathway is a crucial immune-metabolic cascade responsible for either control or explosion of intracellular parasite populations, which is tightly controlled by the Th cell response and the corresponding cytokine environment. Classically activated macrophages (caMΦ), stimulated with TNF-α, IL-12, and IFN-γ, typically referred to as Th1 cytokines, will generate reactive nitrogen species including nitric oxide (NO) and its derivatives NO_2, HNO_2 and $ONOO^-$, *via* the action of inducible nitric oxide synthase (iNOS). By contrast, macrophage exposure to IL-4, IL-13 and IL-21, classically representing Th2 cytokines, stimulates transcription of arginase and the subsequent generation of polyamines via L-ornithine, which support parasite growth and replication. These macrophages are considered as alternatively activated macrophages (aaMΦ).[15,16]

The major underlying immune-metabolic processes of macrophage mediated defense to *L. major* have been described in depth, particularly with regard to the L-arginine pathway and its major metabolic regulators including picolinic acid, an intermediate of the tryptophan degradation (L-kynurenine pathway),[17] phenylalanine and taurine.[18,19] Substantial progress has been made indeed to further dissect the role of selected pathway components, particularly of the role of L-arginine, arginase and iNOS.[16,20−22] However, an approach for simultaneous global metabolic assessment of all participating metabolic entities, that is, parasite, macrophage and cell environment has not been described in depth so far.

Metabolic profiling based on ^{1}H nuclear magnetic resonance (NMR) spectroscopy combined with multivariate modeling strategies and correlation analysis has shown the capacity to shed light on parasite-host interaction *in vivo* in an integrative and nonassumptive way. Despite being applied only in recent years within parasitology, this approach has opened a new avenue to assess parasite-host interplay from a global perspective and allowed unexpected insight into remote parasite effects and systemic metabolic events in the host.[23,24] By coanalyzing and correlating relative cytokine levels with the ^{1}H NMR derived metabolic information, new comprehension on immune-metabolic processes in the host can potentially be obtained.[25,26]

Although *in vivo* research has been the main focus of interest in the field of metabolic profiling, the importance and simplicity of *in vitro* systems has been acknowledged and has offered a simple tool to address more targeted questions. Such research has been introduced more recently as a complementary component in a variety of disease scenarios, including infectious disease and cancer.[27−29]

Here we assess a well-defined cytokine-regulated macrophage *in vitro* system and combine targeted enzymatic and biochemical assays with a ^{1}H NMR-based screening of the single compartments involved, including parasite, external and internal macrophage metabolome, and cell growth supernatant, in order to comprehend the metabolic communication between the metabolically active entities. Three different macrophage activation states were characterized and compared, specifically caMΦ, aaMΦ and nonactivated MΦ (naMΦ) in an uninfected state and during *L. major* exposure. Our studies define the wider metabolic impact of the cytokine induced activation on parasite, macrophage and cell environment.

EXPERIMENTAL PROCEDURES

Culture of Bone Marrow Derived Macrophages

Bone marrow derived macrophages were obtained from naïve 6−8 week old female BALB/c mice (Charles River, U.K.). Bone marrow was harvested by flushing femurs and tibias and 5×10^6 bone marrow precursor cells were differentiated in hydrophobic Teflon bags in 50 mL of macrophage differentiation medium into mature macrophages. The macrophage differentiation medium used was Dulbecco's modified Eagle medium (DMEM, Gibco) supplemented with 10% heat-inactivated fetal calf serum (FCS), 5% horse serum, 50 IU/ml penicillin, 50 μg/mL streptomycin, 2 mM glutamine, (Gibco), 0.05 mM β-mercaptoethanol (SIGMA) and (10% v/v) L929 fibroblast culture supernatant, the latter contains macrophage colony stimulating factor (M-CSF) necessary for the differentiation of the precursor cells into macrophages. The single cell suspensions were differentiated for 8 days in Teflon bags, harvested, washed in DMEM, counted and adjusted to the required cell concentration.

Macrophage Stimulation and Infection

Mature bone marrow derived macrophages (MΦ) were activated in the presence or absence of *L. major* LV39 (MRHO/SU/59/P-strain) promastigotes at a multiplicity of infection of 10 parasites per MΦ. Macrophage cultures were prepared in 6 replicates in 6-well tissue culture plates (Costar) and seeded at 2.5×10^6 cells/well in 5 mL DMEM, supplemented with heat-inactivated 10% FCS, 50 IU/mL penicillin, 50 μg/mL streptomycin, 2 mM glutamine, (Gibco), and 0.05 mM β-mercaptoethanol (SIGMA). Six different groups were assessed and compared, namely alternatively activated macrophages (aaMΦ), classically activated macrophages (caMΦ) and nonactivated macrophages (naMΦ). Each activation state was set up in absence and presence of *L. major* and all cultures were incubated for 48 h at 37 °C, 5% CO_2. The 48 h culture period was selected to ensure optimal viability of macrophages used in the six different groups. Activation stimuli included IFN-γ and TNF-α for caMΦ (5×10^5/mL mature MΦ with 100 U/ml recombinant murine IFN-γ and 500 U/ml recombinant mouse TNF-α; PeproTech) whereas no stimuli were used for naMΦ. IL-4 was supplemented for generation of aaMΦ (5×10^5/mL mature MΦ with 20 U/mL recombinant mouse IL-4 PeproTech).

Parasite Maintenance and Culture

L. major parasites LV39 (MRHO/SU/59/P-strain) were maintained in a virulent state by monthly passage in BALB/c mice. Parasites were isolated monthly from lesions of *L. major* infected BALB/c mice, and used for an average of 6−8 *in vitro* passages. The freshly isolated parasites were cultured and maintained at 26 °C, 5% CO_2 in solid phase blood agar, overlaid with 5 mL DMEM containing 50 IU/ml penicillin and 50 μg/mL streptomycin (P/S). Late log phase/stationary phase *L. major* promastigotes were collected from culture, washed three times in DMEM and an aliquot of the parasite suspension

dx.doi.org/10.1021/pr3003358 | J. Proteome Res. 2012, 11, 4211−4222

was fixed in 2% paraformaldehyde and used for counting parasites using a hemacytometer and adjusted to the required density.

Parasite Transformation

After 48 h of incubation at 37 °C, 10% CO_2 infected macrophages were washed and incubated with freshly prepared sterile lysis medium (DMEM supplemented with 0.008% w/v SDS) for 7−20 min at 37 °C, 10% CO_2. During this time, macrophage disintegration was monitored in regular intervals and when the host cells were lysed, the reaction was stopped by adding DMEM supplemented with 20% heat-inactivated FCS, 20 mM HEPES, 4 mM sodium bicarbonate, 50IU/ml penicillin and 50 μg/mL streptomycin. The lysates containing the liberated *L. major* amastigotes were transferred into blood agar cultures and incubated at 26 °C, 5% CO_2 to allow the amastigotes to transform back into promastigotes and to proliferate. *Leishmania* promastigotes were counted in a separate experiment based on four replicates per activation group, using a hemacytometer after 3−5 days of culture.

For metabolic profile assessment, *L. major* parasites were counted, adjusted to 4.4×10^8 promastigotes and washed three times in ice-cold sterile PBS. Supernatant was removed and the residual parasite pellet was snap frozen on dry ice and subsequently stored at −40 °C prior to NMR analysis.

Preparation of Cell Culture Supernatant and Cell Extracts

A volume of 5 mL of the cell culture medium (= supernatant) was transferred from tissue culture plates into sterile 15 mL Falcon tubes and centrifuged at 2500 rpm at room temperature (RT) to pellet any cell debris. Supernatants were transferred again into a new set of tubes and stored at −40 °C prior to ^{1}H NMR acquisition.

After cell culture medium was removed, macrophage monolayers were quickly washed once with 1 mL/well PBS (kept at RT) which was discarded. This was followed by a cell quenching step using 960 μL of ice cold HPLC grade methanol (Sigma-Aldrich) per well and subsequently placing the plates at 4 °C for 2−5 min to permit cell lysis. Lysed cells and debris were harvested from the bottom of the wells using a cell scraper and the suspension was transferred into 2 mL Eppendorf tubes, whereby the recovered amount was ∼600−650 μL from each well due to the rapid evaporation of the methanol. A further 460 μL methanol were used to rinse each well and subsequently transfer to the cell lysate suspension kept on ice to obtain maximum metabolic yield. Lysates were dried overnight in the SpeedVac at 45 °C, followed by 80% methanol extraction, performed twice, as follows: dried lysates were resuspended in 500 μL cold HPLC grade methanol and vortexed for ∼30 s; 130 μL of distilled water was added into each tube and samples were vortexed again for ∼30 s. Tubes were kept on ice for 10−20 min, spun down at 13000 rpm for 10 min and lysate supernatants transferred into new tubes on ice. Extraction with 80% methanol was performed a second time on the remaining pellets, as described. Tubes were spun down again at 13000 rpm for 10 min. Supernatants were pooled with cell lysate samples from the first methanol extraction and dried overnight in the SpeedVac at 45 °C. Dried cell extracts were stored at −40 °C prior to preparation for ^{1}H NMR analysis.

^{1}H NMR Spectroscopic Assessment

Equal amounts of cell supernatant and phosphate buffer (0.2 M Na_2HPO_4, 0.043 M NaH_2PO_4, D_2O:H_2O = 7:3, v/v, 0.01% of sodium 3-(trimethylsilyl) propionic acid 2,2,3,3-d4 ([TSP)], pH = 7.4), were mixed to a total amount of 600 μL in Eppendorf tubes by vortexing. Samples were spun down at 13000 rpm for 5 min and 550 μL was transferred into 5 mm NMR tubes.

Cell extracts were resuspended in 600 μL phosphate buffer via vortexing. Samples were spun down at 13000 rpm for 5 min and 550 μL of the supernatant was transferred into 5 mm NMR tubes.

A frozen pellet of 4.4×10^8 parasites was transferred immediately into a ZrO_2 rotor and ∼25 μL D_2O were added. After inserting a spacer to adjust for the small amount of biomass, the rotor was sealed with a Kel-F rotor cap.

All cell culture supernatants were assessed on a Bruker Avance 600 NMR spectrometer with TXI probe head (Bruker; Rheinstetten, Germany) operating at 600.13 MHz for proton frequency, whereby 128 scans per sample were sufficient for obtaining optimal signal output.

The cell extracts were acquired using a cryo probe head (CO TCI) in order to minimize electric noise and augment the signal-to-noise ratio, whereby the number of scans was adjusted to 384 for each sample. A standard 1-dimensional (1D) pulse program was applied (recycle delay (RD)-90°-t1-90°-tm-90°-acquisition time (AQ)) and the water impact on the baseline was minimized by irradiating the water frequency during the RD (2 s). The 90° pulse length was set to 14.75 s for all cell supernatants and 14.62 s for the cell extracts. The spectra were recorded in 32768 data points within a spectral width of 20 ppm and a 0.3 Hz line-broadening factor was applied to the free induction decays (FIDs) prior to Fourier transformation.

In contrast to supernatants and cell extracts, the *L. major* pellet was acquired via high resolution magic angle spinning (MAS)-NMR to maximize metabolic information from such a small amount of biomass.[30] The rotor was therefore placed in a MAS probe at an angle of 54.7° and spun at 5000 kHz in order to compensate for the line broadening effects introduced by the restricted motion of the analyte and the sample heterogeneity. Additionally to 1D spectral acquisition, a Carr−Purcell−Meibom−Gill (CPMG)[31] pulse sequence was applied to the parasite pellet in order to account for the smaller metabolic weight components. MAS spectra were acquired in 256 scans and recorded in 65536 data points, whereby a 90° pulse length of 10.43 s was applied. All other parameters remained the same as described above.

Spectral assignments were made by consulting the literature and in-house databases confirmed via statistical total correlation spectroscopy (STOCSY)[32] and using NMR suite profiler software (Chenomx, USA).

Data Processing and Statistical Treatment

Spectral data were processed using nmrproc, an in-house developed MATLAB algorithm (Dr. Tim Ebbels and Dr. Hector Keun, MathWorks) which performs optimized phasing, baseline alignment and automatic calibrating to the TSP reference peak at δ 0.00. To exclude the reference peak and residual resonances of the water peak from the data modeling process, only the spectral region from δ 0.5−9 was imported into MATLAB and the region affected by the water was cut out, that is, δ 4.54−4.98 for extracts and δ 4.7−5 for the supernatants. An in house adapted script for probabilistic quotient normalization was applied prior to statistical analysis (Dr. Kirill Veselkov).[33,34]

Multivariate analysis including principal component analysis (PCA) and partial least-squares (PLS)-related methods were

dx.doi.org/10.1021/pr3003358 | J. Proteome Res. 2012, 11, 4211−4222

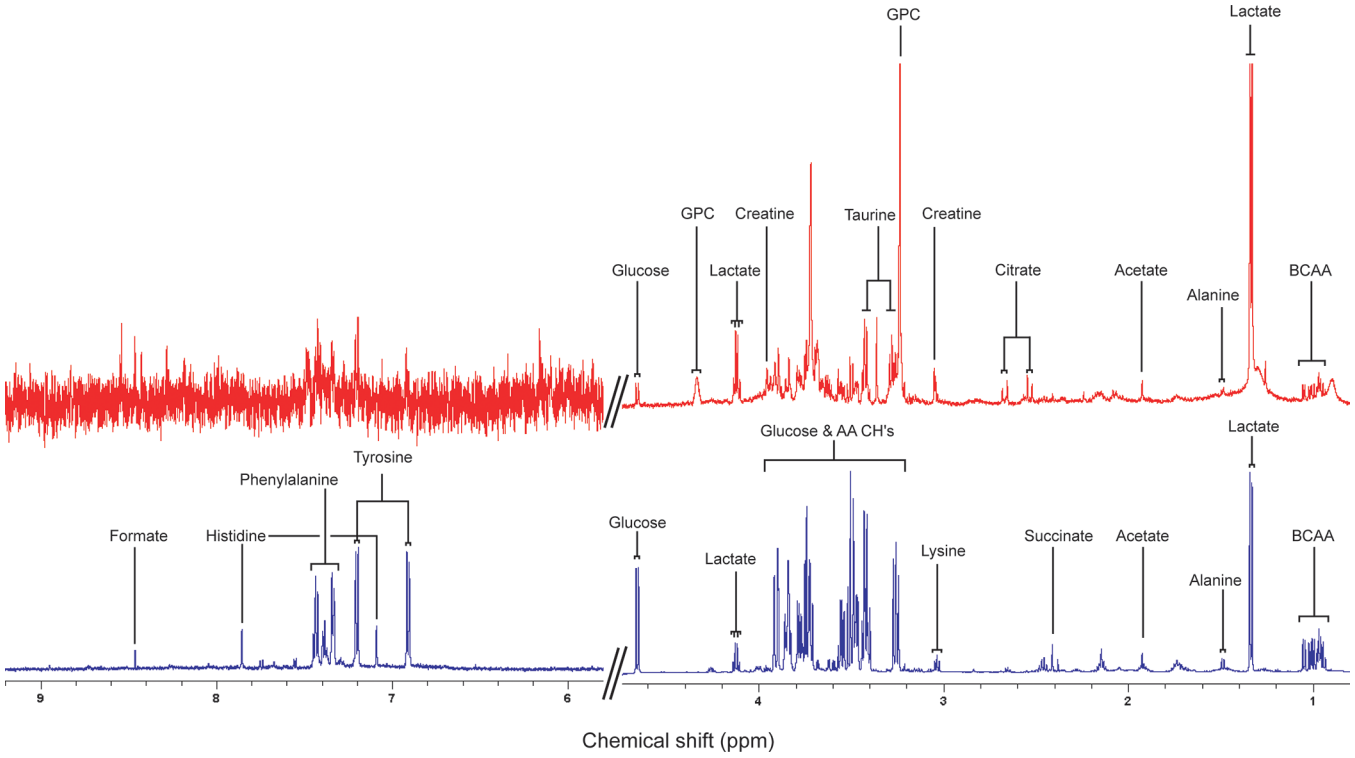

Figure 1. [1]H NMR spectrum of cell extract acquired by using a standard pulse sequence on cell extracts (red) and cell culture supernatants (blue). The metabolite concentration differes substantially between the two matrixes assessed which leads to a generally lower signal-to-noise ration in the spectra acquired from the cell extracts. Key: AA's, amino acids; BCAA, branched chain amino acids; GPC, glycerophosphocholine.

applied to the data using a SIMCA (Umetrics, Sweden) and MATLAB interface. As unsupervised method, PCA offers an unbiased overview on the general data distribution of a data matrix (X) by compressing the total amount of information into one single data point onto a plane.[32,35] The resulting scores plot allows visualization of groupings, outliers and time trajectories hence PCA is the ideal tool for defining further analytical strategy. PLS on the other hand relates the data in X to a second matrix (Y) containing a separate set of information which can be quantitative, such as cytokine levels, parasitaemia, inflammatory markers, etc., or qualitative (e.g., affiliation to class) in which case a PLS discriminant analysis (PLS-DA) would be applied.[35,36] O-PLS-DA is a further optimization and is currently being applied for biomarker identification, comparing two classes of samples.[37,38] Whereas the PLS algorithm maximizes the class differences and facilitates identification of the loadings (metabolites) responsible, the inbuilt orthogonal filter removes systemic variation unrelated to class-affiliation.

Additional univariate approaches have been applied to further evaluate the candidate biomarkers. Integrals from selected nonoverlapped regions from each potential biomarker were therefore calculated in MATLAB and imported into GraphPad PRISM (GraphPad, USA) and SPSS (IBM Corporation, USA) for graphical representations and univariate statistical tests which included two tailed Mann–Whitney U-test with Bonferroni correction for pair wise comparison and Kruskal–Wallis for multiple group comparisons.

Arginase Activity

In addition to the 6 well cultures for metabolic profiling, macrophage cultures (1 mL/well) were set up in four replicates in 24 well tissue culture plates and stimulated and infected in parallel. Bone-marrow derived macrophages (5×10^5/mL) were assessed in unstimulated, classically, and alternatively activated state (as above) in the absence or presence of *L. major* promastigotes at a multiplicity of infection (MOI) of 10:1. After 48 h of culture at 37 °C, 10% CO_2, macrophages were washed and lysed.

Arginase activity was measured in macrophage lysates by measuring the conversion of L-arginine to urea, as described previously.[16,39] Briefly, cells were lysed with 0.1% Triton X-100 (Sigma) and 50 mM Tris-HCl (pH 7.5, Sigma), which contains the arginase cofactor manganese chloride (Sigma) and the enzyme activated at 56 °C for 7 min. The hydrolysis was conducted by the addition of 0.5 M L-arginine (pH 9.7) and incubated at 37 °C for 15–120 min. The reaction was stopped using an acid mix consisting of phosphoric acid (85%, Fluka), sulphuric acid (98%, Fluka) and distilled water at a v/v/v ratio of 1/3/7. The urea production via the hydrolysis of L-arginine by arginase was measured by the addition of 6% α-isonitrosopropiophenone and incubated at 100 °C for 45 min. Urea production by L-arginine hydrolysis in samples was measured against a urea standard and the OD of the reactions was measured at 550 nm. Arginase activity was calculated in mU per sample and expressed per 1×10^6 macrophages, whereby the lowest detectable level of arginase was 2.1 mU/1×10^6 macrophages. One unit of enzyme activity defined as the amount of enzyme that catalyzes the formation of 1 μM urea per minute.

Nitrite Production

After two days at 37 °C, 10% CO_2, culture supernatants were harvested from the different macrophage cultures in 24 well plates. Nitrite accumulation was used as an indicator of nitric oxide (NO) production in culture supernatants and measured

dx.doi.org/10.1021/pr3003358 | J. Proteome Res. 2012, 11, 4211–4222

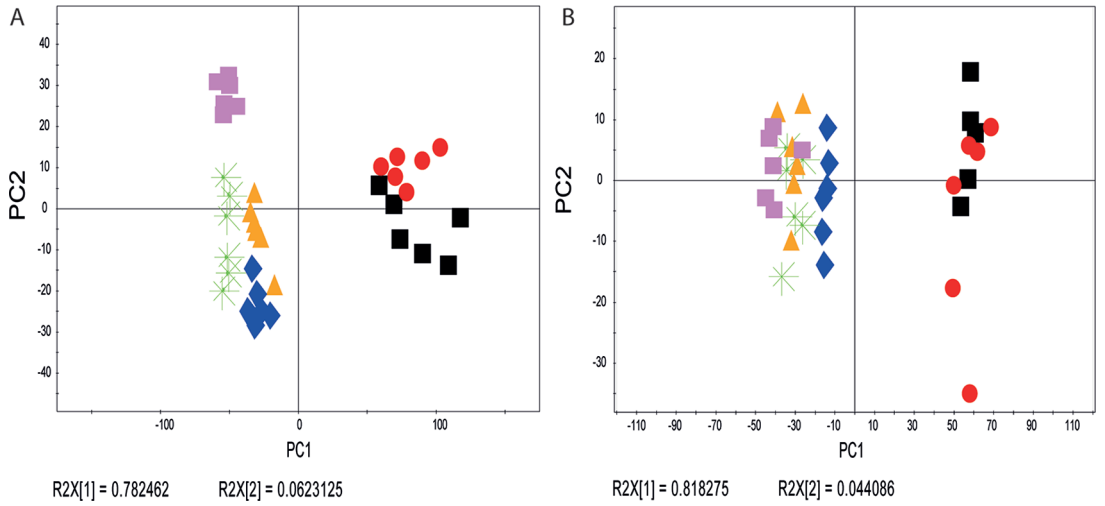

Figure 2. PCA analysis of (A) cell extracts and (B) cell supernatants. The groups in the scores plots represent different infection and activation states of the bone marrow derived macrophages. R2X explaines the variance in the model for each component. Key: blue, aaMΦ infected; green, aaMΦ uninfected; yellow, naMΦ infected; pink, naMΦ uninfected; red, caMΦ infected; black, caMΦ uninfected.

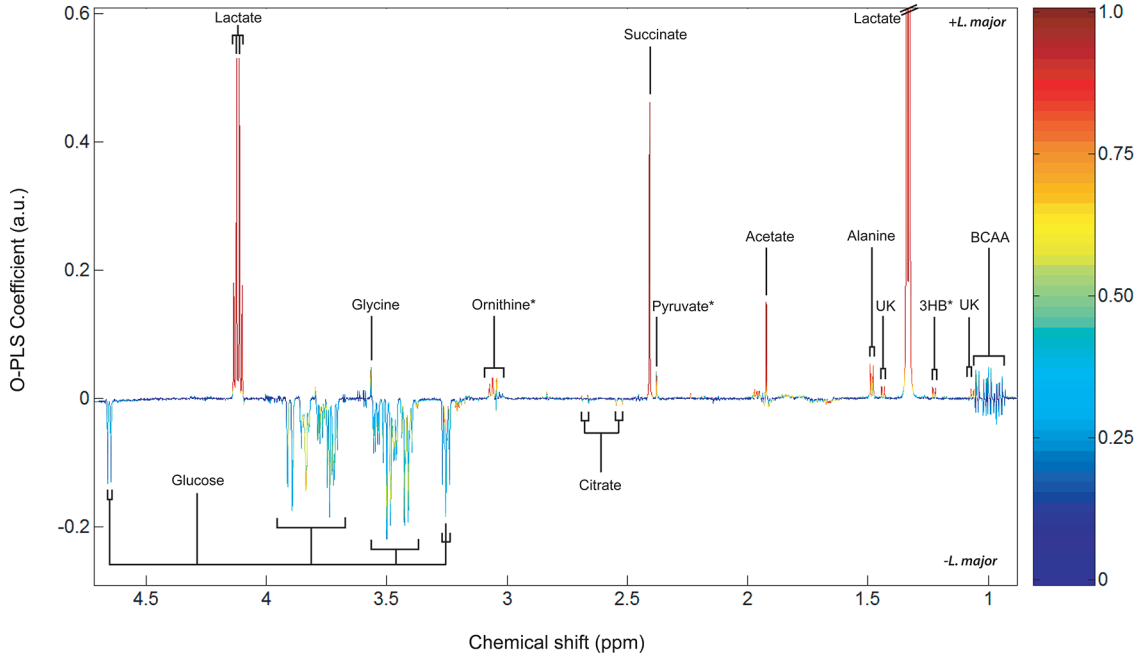

Figure 3. O-PLS-DA analysis comparing spectra of cell supernatants of infected and uninfected aaMΦ. Metabolites which are different between the two states are color coded according to significance, whereby red denotes highest and blue no discriminatory power. Upward pointing peaks are positively correlated with the infection, whereas downward pointing peaks are anti correlated with *L. major* infection. Key: a.u., arbitrary units; BCAA, branched chain amino acids; 3HB, 3-hydroxybutyrate; UK, unknown metabolite; *, tentatively assigned.

by using the Griess reagent. Equal volumes of macrophage culture supernatants and Griess reagent (1% sulphanilamide/0.1% *N*-(1-naphtyl) ethlyenediamine dihydrochloride/2.5% H_3PO_4) were incubated at room temperature for 10 min. Absorbance was measured in a microplate reader at 550 nm. Nitrite concentration was determined using $NaNO_2$ as standard. The limit of detection was set at 5 μM nitrite.

RESULTS

Global Data Distribution and Biomarker Identification

Spectral data from macrophage extracts and cell supernatants (Figure 1) were assessed separately for differences between infection and activation state. PCA of cell extract spectra revealed clear groupings between the different macrophage activation states as well as between *L. major* infected and uninfected cell cultures (Figure 2A). The most striking separation was observed between caMΦ and all other *in vitro* conditions. Analysis of the cell culture supernatants also indicated a metabolic separation between the activation states along the first principal component (PC1), again showing a distinction between caMΦ from all other data points (Figure 2B). Infection induced a shift of the aaMΦ data points along PC1 but no clear infection-related group separation was found within caMΦ and naMΦ spectra.

To identify the metabolites responsible for group separation O-PLS-DA was applied in a first step (Figure 3). To further validate the statistical significance of the identified metabolic

dx.doi.org/10.1021/pr3003358 | *J. Proteome Res.* 2012, 11, 4211−4222

Table 1. Discriminating Metabolites Associated with *L. major* Infection[a]

		caMΦ's		aaMΦ's		naMΦ's	
	Metabolite	Fold change relative to noninfected	*p*	Fold change relative to noninfected	*p*	Fold change relative to noninfected	*p*
Cell culture supernatants	Acetate	0.32	**	0.32	**	0.32	NS
	Alanine	0.07	*	0.07	**	0.07	NS
	Citrate	0.02	NS	0.02	*	0.02	NS
	Fumarate	0.65	*	0.65	*	0.65	NS
	Glucose	−0.06	NS	−0.06	**	−0.06	NS
	Lactate	−0.01	NS	−0.01	**	−0.01	NS
	Ornithine	−0.04	NS	−0.04	**	−0.04	NS
	Pyruvate	0.28	**	0.28	**	0.28	NS
	Succinate	0.84	**	0.84	**	0.84	*
Cell Extracts	Acetate	−0.10	NS	−0.10	**	−0.10	**
	β-Alanine	0.05	NS	0.05	*	0.05	**
	Citrate	−0.10	NS	−0.10	*	−0.10	**
	Creatine	0.53	**	0.53	**	0.53	**
	Creatine Phosphate	0.14	NS	0.14	**	0.14	**
	Glycerophosphocholine	0.03	NS	0.03	**	0.03	**
	Glycine	0.01	NS	0.01	NS	0.01	**
	Lactate	−0.18	NS	−0.18	**	−0.18	**
	Phosphocholine	−0.15	NS	−0.15	**	−0.15	**
	Taurine	0.04	NS	0.04	NS	0.04	**

[a]Metabolites were selected based on the O-PLS-DA output and the difference in between the median values of metabolite concentrations (in mM, estimated from integral calculations, relative to TSP) between infected group and non-infected group was calculated for each. Changes in median concentration and fold changes were calculated relative to non-infected states, whereby increases are shown as positive values and decreases are shown as negative values. Statistical significance (p) measured *via* two-tailed Mann-Whitney test (with Bonferroni correction for individual MΦ subsets) whereby *, $p < 0.05$; **, $p < 0.01$; ***, $p < 0.001$; ****, $p < 0.0001$; and NS, not statistically significant.

Table 2. Discriminating Metabolites in the Cell Culture Supernatant Associated with Macrophage Activation[a]

	noninfected MΦ's				*L. major*-infected MΦ's			
	Median concentration and range (mM)				Median concentration and range (mM)			
Metabolite	CA	AA	NA	*p*	CA	AA	NA	*p*
Acetate	0.152 (0.148−0.159)	0.136 (0.129−0.139)	0.168 (0.157−0.212)	***	0.200 (0.195−0.220)	0.169 (0.166−0.169)	0.209 (0.174−0.210)	**
Alanine	0.887 (0.853−0.924)	1.002 (0.956−1.022)	1.016 (0.946−1.054)	**	0.945 (0.932−1.029)	1.079 (1.065−1.086)	1.072 (1.045−1.098)	**
Citrate	0.126 (0.122−0.154)	0.161 (0.152−0.169)	0.128 (0.124−0.141)	**	0.128 (0.124−0.141)	0.153 (0.150−0.157)	0.137 (0.126−0.141)	**
Glucose	10.261 (9.276−10.717)	15.701 (14.437−15.179)	15.609 (14.701−16.663)	**	9.670 (9.070−10.523)	13.848 (13.524−13.977)	15.067 (14.825−16.540)	**
Glycine	0.289 (0.273−0.296)	0.308 (0.305−0.320)	0.329 (0.313−0.343)	**	0.276 (0.269−0.302)	0.314 (0.311−0.325)	0.329 (0.328−0.336)	***
Lactate	8.149 (7.734−8.791)	2.018 (1.830−2.119)	1.551 (1.503−2.244)	***	8.048 (7.684−8.864)	3.228 (3.069−3.350)	2.231 (1.447−2.278)	***
Ornithine	0.216 (0.210−0.239)	0.361 (0.330−0.376)	0.226 (0.211−0.237)	**	0.209 (0.203−0.234)	0.395 (0.384−0.399)	0.226 (0.218−0.233)	***
Pyruvate[b]	0.095 (0.087−0.103)	0.073 (0.070−0.076)	0.097 (0.095−0.105)	**	0.121 (0.111−0.132)	0.081 (0.078−0.086)	0.097 (0.92−0.98)	***
Succinate	0.091 (0.088−0.095)	0.090 (0.085−0.092)	0.094 (0.088−0.192)	NS	0.167 (0.162−0.181)	0.186 (0.182−0.192)	0.193 (0.097−0.196)	*

[a]Metabolite levels are displayed as median concentration and range per condition (in mM), estimated from integral calculations, relative to TSP. Statistical significance (p) measured *via* Kruskal-Wallis test across three activation classes, whereby *, $p < 0.05$; **, $p < 0.01$; ***, $p < 0.001$; and NS, not statistically significant. [b]Tentatively assigned.

markers, the integrals were calculated for each, and subjected to univariate nonparametric tests (see methods). In Table 1, those metabolites are represented that were found to be statistically different between infected and noninfected samples, whereas Tables 2 and 3 show the metabolic differences between activation states, that is, aaMΦ, caMΦ and naMΦ. Only metabolites that reached statistical significance as validated via uni- and multivariate methods are documented.

The infection state showed particular discrimination in cell culture supernatants of aaMΦ and the cell extracts of naMΦ (Table 1), whereas the naMΦ supernatants did not appear to differ significantly between the infected and uninfected state with the exception of increased succinate after *L. major*

dx.doi.org/10.1021/pr3003358 | J. Proteome Res. 2012, 11, 4211−4222

Table 3. Discriminating Metabolites in Cell Extracts Associated with Macrophage Activation[a]

	noninfected MΦ's				*L. major*-infected MΦ's			
	Median concentration and range (mM)				Median concentration and range (mM)			
Metabolite	CA	AA	NA	*p*	CA	AA	NA	*p*
Acetate	0.012 (0.011−0.014)	0.010 (0.009−0.012)	0.010 (0.007−0.010)	**	0.011 (0.009−0.012)	0.014 (0.013−0.015)	0.013 (0.011−0.014)	**
β-Alanine	0.028 (0.021−0.029)	0.027 (0.023−0.039)	0.012 (0.011−0.014)	**	0.029 (0.020−0.034)	0.052 (0.031−0.056)	0.035 (0.023−0.036)	**
Citrate	0.045 (0.035−0.048)	0.024 (0.019−0.032)	0.015 (0.010−0.016)	***	0.040 (0.035−0.050)	0.032 (0.030−0.037)	0.028 (0.026−0.057)	*
Creatine	0.021 (0.017−0.023)	0.022 (0.014−0.025)	0.006 (0.004−0.006)	**	0.032 (0.025−0.043)	0.055 (0.046−0.058)	0.026 (0.023−0.030)	**
Creatine Phosphate	0.012 (0.010−0.015)	0.026 (0.015−0.028)	0.005 (0.004−0.006)	***	0.013 (0.011−0.015)	0.055 (0.050−0.057)	0.026 (0.020−0.029)	***
Glucose	0.080 (0.068−0.146)	0.123 (0.094−0.162)	0.093 (0.114−0.217)	NS	0.057 (0.042−0.088)	0.099 (0.068−0.134)	0.115 (0.165−0.261)	**
Glycerophosphocholine	0.074 (0.061−0.082)	0.010 (0.007−0.012)	0.007 (0.006−0.008)	***	0.077 (0.056−0.091)	0.027 (0.022−0.028)	0.026 (0.024−0.029)	**
Glycine	0.010 (0.008−0.012)	0.008 (0.006−0.021)	0.007 (0.004−0.007)	*	0.010 (0.005−0.028)	0.010 (0.009−0.013)	0.010 (0.009−0.011)	NS
Lactate	0.153 (0.140−0.247)	0.055 (0.038−0.071)	0.031 (0.018−0.034)	***	0.126 (0.096−0.142)	0.090 (0.075−0.104)	0.063 (0.049−0.083)	**
Phosphocholine	0.014 (0.007−0.016)	0.007 (0.004−0.007)	0.003 (0.003−0.003)	***	0.012 (0.010−0.019)	0.012 (0.011−0.013)	0.010 (0.009−0.012)	NS
Taurine	0.127 (0.098−0.163)	0.206 (0.129−0.224)	0.108 (0.087−0.132)	**	0.132 (0.100−0.145)	0.211 (0.182−0.226)	0.207 (0.174−0.232)	**

[a]Metabolite levels are displayed as median concentration and range per condition (in mM), estimated from integral calculations, relative to TSP. Statistical significance (p) measured *via* Kruskal-Wallis test across three activation classes, whereby *, $p < 0.05$; **, $p < 0.01$; ***, $p < 0.001$; and NS, not statistically significant.

exposure. The caMΦ cell extracts did not seem to undergo major metabolic changes either upon infection and showed solely an increase of creatine. The cell supernatants on the other hand revealed elevated levels of acetate, alanine, fumarate, pyruvate and succinate in those samples which have been incubated with *L. major*.

The activation state was reflected strongly in the metabolic background, that is, cell extracts and culture supernatant in both *L. major* infected and uninfected macrophage cultures (Tables 2 and 3). A depletion of glucose, alanine, and glycine (cell culture supernatant) and a subsequent increase of lactate (cell culture supernatant or extract) was the most general change comparing caMΦ with either naMΦ or aaMΦ in both states, infected and uninfected (Tables 2 and 3, Figures 3 and 4). More specific differences included relative lower acetate levels in aaMΦ cell supernatants compared to naMΦ supernatants during infection, or a general higher intracellular level of taurine in both aaMΦ and naMΦ compared to caMΦ during infection.

A few biomarkers that were identified in the cell culture supernatants were also found in the cell extracts, namely acetate, citrate and lactate, whereas others were specific to extracts (e.g., creatine, creatine phosphate and choline derivatives) and supernatants (e.g., succinate, alanine) (Tables 1−3), which is in line with the general metabolite recovery (Table 4).

Metabolic Characterization of *In Vitro* Compartments

The metabolites detected by ^{1}H NMR spectroscopy of macrophage extracts, macrophage culture supernatants, fresh cell culture growth media and *L. major* showed a high overlap. A list of metabolites identified in each compartment is presented in Table 4. Lactate and the branched chain amino acids (BCAA) leucine, isoleucine and valine, were identified in all four compartments, and a large amount of metabolites was observed in three compartments, including acetate, glucose, glycine, phenylalanine and tyrosine. Uracil on the other hand was only present in the *L. major* metabolome and formate and fumarate were specific to the external macrophage metabolome (Figures 1 and 5 and Table 4). Some residual lipid resonances were observed only in MAS NMR spectra of *L. major* (Figure 5) as a result of analyzing intact parasites and not further discussed in comparisons to solution-state analyses of cell extracts which focused only on polar metabolites. Alanine, acetate, citrate, succinate, 3-hydroxybutyrate, formate and fumarate were all found in the supernatant after incubation with cellular material.

L-Arginine Metabolism and Parasite Replication

Arginase activity, NO production and parasite counts were assessed in two separate experiments including four replicates in order to confirm that the different stimulation assays resulted in the expected macrophage activation state and the expected effect to infection intensity. The nitric oxide assay did not show detectable amounts of NO in naMΦ and aaMΦ (limit of detection 5 μM) but revealed higher levels in *L. major* infected cells (76.1 ± 4.38 μM) compared to the uninfected control samples (58.1 ± 1.99 μM) as validated by the nonparametric Mann−Whitney U test ($p < 0.05$).

Pronounced arginase activity was detected in aaMΦ (*L. major* (−): 580.8 ± 16.40; *L. major* (+): 666.0 ± 2.06 mU/10^6 cells), whereas naMΦ (*L. major* (−): 17.6 ± 0.29; *L. major* (+): 21.1 ± 0.17 mU/10^6 cells) and caMΦ (*L. major* (−): 6.7 ± 1.59; *L. major* (+): 47.8 ± 0.78 mU/10^6 cells) only expressed background levels of arginase activity. Significance of the effect was confirmed *via* Kruskal−Wallis test ($p < 0.01$). Additional

dx.doi.org/10.1021/pr3003358 | *J. Proteome Res.* 2012, 11, 4211−4222

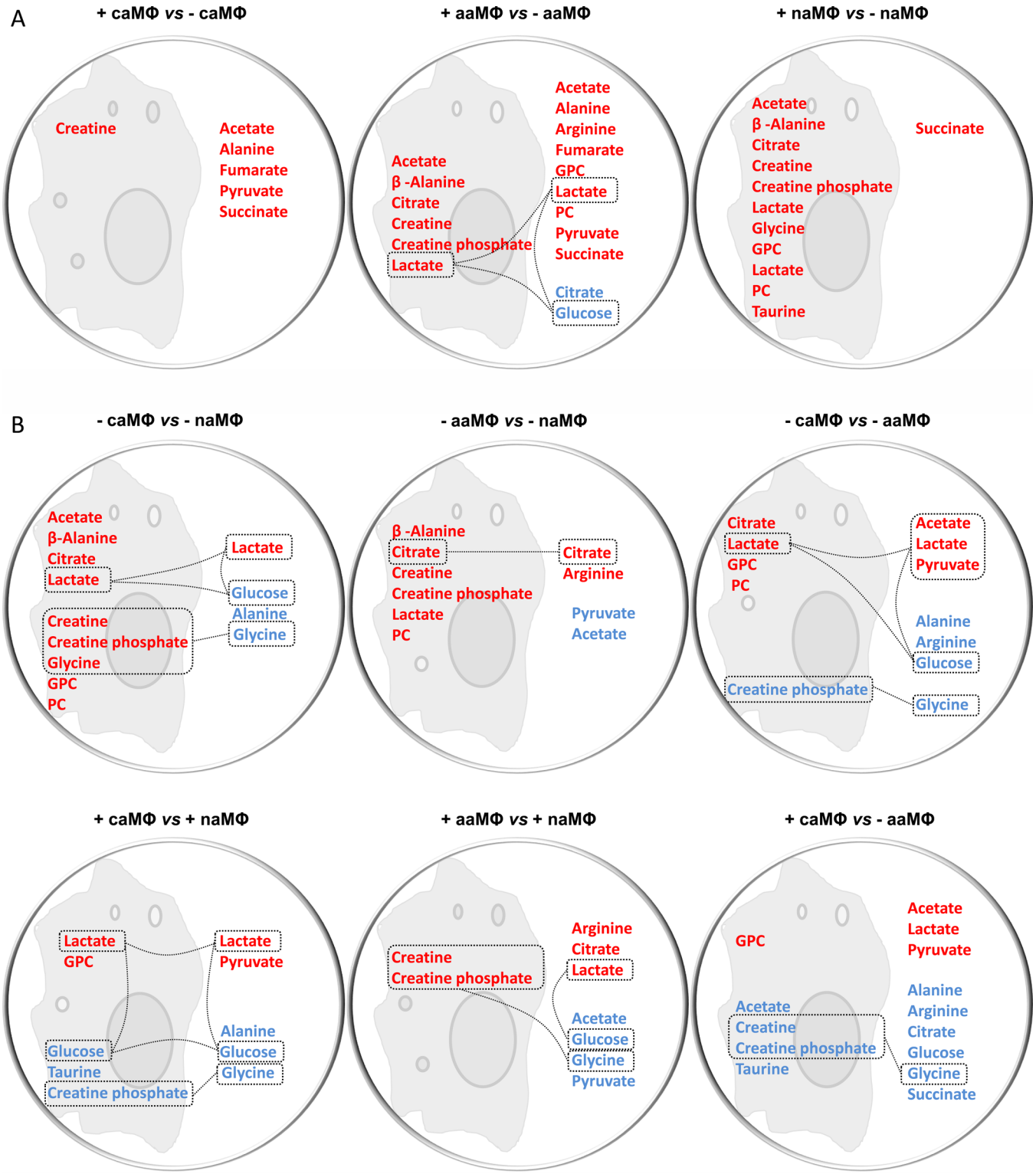

Figure 4. Biomarkers represented in a schematic *in vitro* context arranged in pairwise comparisons: Those metabolites within the macrophage were identified as biomarkers derived from the analysis on the cell extracts, whereas the metabolites outside the cell denote changes characterized in the corresponding cell supernatants. A) Effect of infection within each activation state, whereby metabolites in red indicate a relative increase of the metabolite during infection whereas blue metabolites were found to be relatively lower in macrophages infected with *L. major*. B) Effect of activation state within uninfected cells (top row) and infected macrophages (bottom row). The color code (red, increased; blue, decreased) referes to the first mentioned activation state in each pairwise comparison, for example, in caMΦ vs naMΦ, the red metabolites would refer to caMΦ, indicating that in caMΦ red is relatively increased compared to naMΦ, etc. Key: +, infected with *L. major*; −, uninfected control cells.

Mann−Whitney tests between infection and control groups within each activation class revealed that NO and arginase activity were significantly different between infected and uninfected MΦ throughout all activation groups in which detectable levels were obtained. Whereas NO was found to be relatively higher in *L. major* (+) caMΦ than in *L. major* (−)

dx.doi.org/10.1021/pr3003358 | *J. Proteome Res.* 2012, 11, 4211−4222

Table 4. Metabolites Identified via ^{1}H NMR Spectroscopy in *L. major*, Macrophage Extracts (Internal Metabolome), Macrophage Culture Supernatant (External Metabolome) and Pure DMEM, to Compare Overlap of Metabolic Information between the Compartments[a]

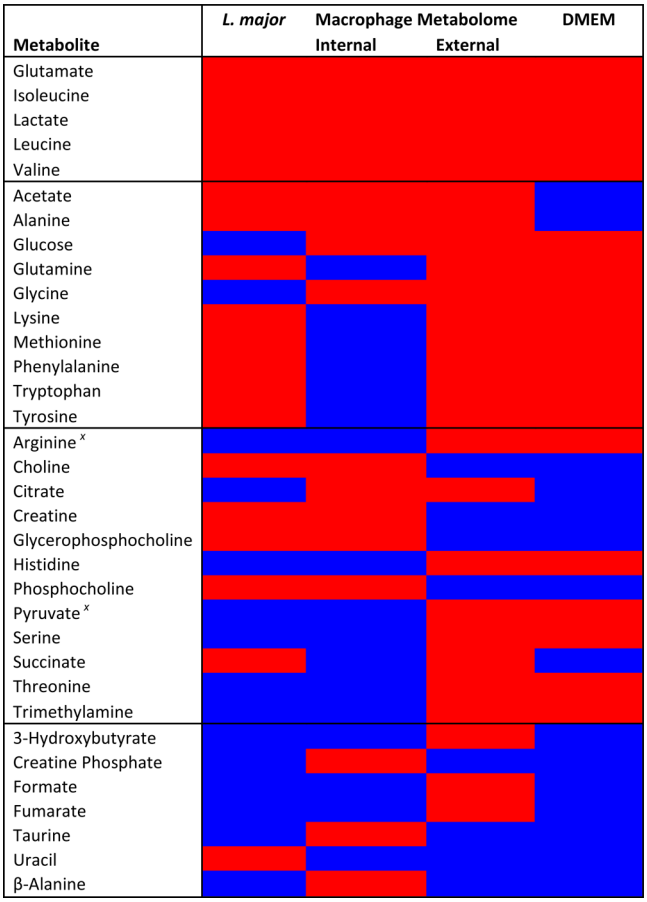

[a]The color code indicates presence (red) and no confirmed detection of a metabolite (blue). GPC, Glycerophosphocholine; *x*, tentatively assigned.

caMΦ, arginase levels were significantly higher in *L. major* (+) aaMΦ and naMΦ compared to each corresponding uninfected set of cells but were found to be relatively lower in *L. major* (+) caMΦ compared to *L. major* (−) caMΦ.

Parasite transformation and determination of promastigote survival after 48 h intracellular exposure to the different activation states confirmed the well established association of NO with parasite killing and arginase with promotion of parasite growth. About 70% fewer promastigotes were recovered from caMΦ ($5 \times 10^6 \pm 0.66 \times 10^6$) whereas higher promastigote numbers were recovered from aaMΦ ($28.3 \times 10^6 \pm 3.12 \times 10^6$) as compared to baseline levels in naMΦ ($22.8 \times 10^6 \pm 1.32 \times 10^6$). The parasite decrease in caMΦ was confirmed as significant by the nonparametric Kruskal–Wallis test between all three activation groups.

DISCUSSION

Macrophage activation plays a critical role in determining disease progress during the course of *L. major* infection. Whereas classical activation leads to clearance of the parasite via generation of reactive nitrogen species, in particular NO, alternative activation will induce increased arginase-mediated conversion of L-arginine to ornithine and polyamines, which are used as substrates for parasite growth and replication.[15,16,20] The measured NO production and arginase activity in the here presented study confirmed that the different stimulation conditions used, resulted in alternatively or classically activated macrophages. The parasite counts furthermore confirmed the leishmanicidal effect of the classical activation pathway products. The metabolic screening of cell extracts via ^{1}H NMR has revealed clear metabolic differences between aaMΦ's, caMΦ's and naMΦ's in *L. major*-infected and uninfected state, whereby the classical activation state separated most clearly from all other conditions. The corresponding cell culture supernatant confirmed the striking separation of the caMΦ's from all other states in the global PCA (Figure 2), indicating that classical activation of the macrophages has a more profound effect on the global cellular metabolism than the coexistence of an intracellular pathogen. The more obvious group separation of *L. major*-exposed cells in the extracts, compared to the cell supernatants, might be due to the exposure of any secreted components to the relatively large volume of external growth medium. A potential dilution of cell derived metabolites might render the detection of more subtle changes to intracellular metabolic pathways more difficult in the extracellular milieu. However, subsequent in depth analysis using O-PLS discriminant analysis was able to detect those subtle differences and reveal the biomarkers responsible for discrimination of infection and activation state. Moreover the biomarker yield in each compartment was dependent on activation state but overall quantitatively comparable (Figure 4).

O-PLS-DA assessment of infection markers within each of the three activation states separately, showed that *L. major* infection induced a similar metabolic fingerprint in all macrophage populations, which included different combinations of relatively elevated levels of actetate, alanine, pyruvate, succinate and lactate in internal and external macrophage metabolome and may, as main end products of *Leishmania*, reflect a direct contribution of the parasite (Figures 3 and 4, Table 1).[2,40]

The strongest biomarkers that were recovered from the analysis of the macrophage extracts included glycerophosphocholine, phosphocholine, creatine phosphate and creatine which were measured at relative higher concentrations in infected samples from aa and naMΦ, compared to the noninfected corresponding samples (Figure 4; Table 1). The increase of choline species might indicate a certain degree of membrane decomposition and subsequent lipid degradation during invasion of *L. major*,[41] which did not seem to have been the case after classical activation. The higher cellular uptake of creatine (aa, ca. and naMΦ's) and creatine phosphate (aa and naMΦ's), on the other hand might reflect the higher energy demand of the macrophages in order to cope with the infection, since creatine phosphate represents a major cellular short-term energy reserve for ATP generation.[42] The caMΦ showed, however, overall the least metabolic differences between *L. major*-infected and uninfected state, which may be explained by the confirmed effective intracellular killing of the parasite and hence a relatively minor accumulation of metabolic end products and intracellular pathway interruptions in contrast to the uncontrolled growth and replication of *L. major* in naMΦ and aaMΦ. Parallel evaluations of arginase and NO indeed confirmed relatively higher leishmanicidal activity and significantly lower parasite counts in caMΦ.

dx.doi.org/10.1021/pr3003358 | J. Proteome Res. 2012, 11, 4211–4222

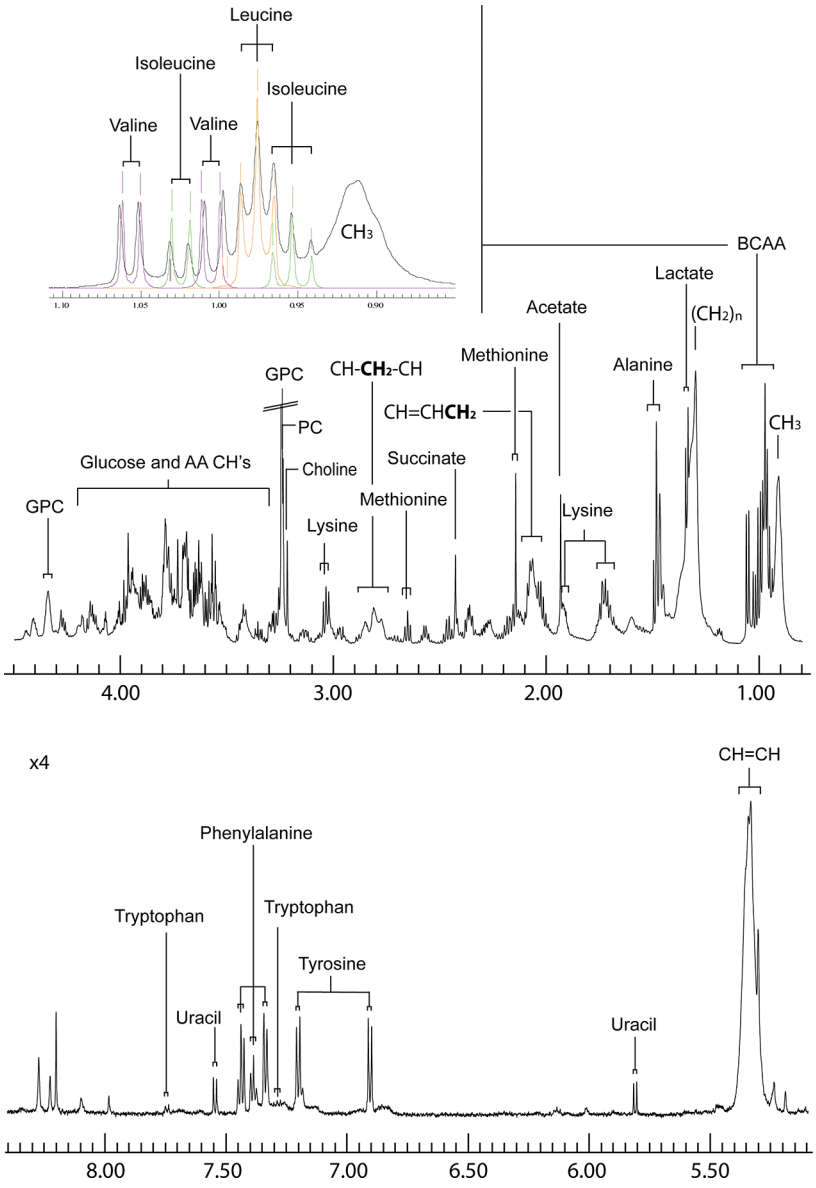

Figure 5. High resolution ^{1}H MAS NMR acquisition of *L. major* pellet using a cpmg pulse sequence to obtain overview on the small metabolic weight components of the parasite. The top figure indicates the alphatic region of a ^{1}H NMR spectrum and the bottom represents CH groups in aromatic systems. The standards for the BCAA assignements were used and overlapped in Amix, Version 3.9.3. Key: AA, Amino acid; BCAA, Branched chain amino acid; GPC, Glycerophosphocholine; PC, Phosphocholine.

The most striking effect related to macrophage activation state was the clear separation of the caMΦ's from both aa and naMΦ's (Figure 2, Tables 2 and 3). Biomarker assessment within each infection state (*L. major* present and absent) revealed that a depletion of glucose in the cell culture supernatants and a subsequent increase of lactate in both macrophage extract and culture supernatants were the main metabolic drivers for the separation and indicate that caMΦ has a significantly higher energy demand compared to the other two groups, to successfully defend infection. An increased amount of ATP is necessary, for instance, for enzyme activity such as the NADPH oxidase which is crucial for the production of reactive oxygen and nitrogen species.[43] It has been shown that the excessive NO production upon classical activation can lead to complete arrest of ATP production via the respiratory chain. Anaerobic glycolysis therefore undergoes an increase to meet the ATP demand in the macrophage.[44] The increased glycolytic rate and the subsequent accumulation of lactate, in turn, might be directly responsible for the observed pH decrease in the cell supernatants of infected caMΦ (caMΦ 6–7; aa and naMΦ's 8–9). The potential contribution of parasitic D-lactate[40] seems herby unlikely, since no lactate increase was observed in infected caMΦ compared to uninfected samples (Figure 4, Table 1).

The majority of metabolites which were found prevalent in all or most compartments assessed were amino acids and glucose to serve as source for energy and anabolic pathways. Choline and its derivatives phosphocholine and glycerophosphocholine (GPC), on the other hand, were found in the intracellular metabolome of parasite and macrophage but not in the external fluids, which might reflect accumulation of the intermediates for the intracellular recycling process of remodelling the cell membrane, since choline is substrate for the phospatidylcholine anabolism.[41,45]

dx.doi.org/10.1021/pr3003358 | *J. Proteome Res.* 2012, 11, 4211–4222

The tricarboxylic acid cycle intermediates citrate, fumarate, pyruvate and succinate were unequally distributed throughout the compartments whereby presence in the external macrophage metabolome was the only commonality. Only succinate was detected in the protozoa via ^{1}H NMR, which might reflect back to the fact that the compound is one of the main metabolic end products of *L. major* with relatively higher accumulation in the parasite when compared with fumarate and citrate for instance.[2,40]

The culture growth medium and the external macrophage metabolome showed the highest degree of intercompartment overlap (i.e., 79.4%). Qualitative differences were detected in only 7 out of 34 metabolites and include acetate, alanine, citrate, succinate, 3-hydroxybutyrate, formate and fumarate which were all present in the macrophage footprint but absent in pure DMEM. Whereas acetate, alanine and succinate are major end products of the *Leishmania* metabolism and might be directly derived from the parasite, the remaining components are likely to reflect metabolic waste products of both, macrophage and parasite metabolism.

CONCLUSION

Work in previous parasite-rodent models has shown the capacity of metabolic profiling in discovery of infection-specific candidate diagnostic biomarkers and in characterizing immune-metabolic codevelopment during infection. Whereas *in vivo,* immune measures such as cytokines are being coanalyzed with the metabolic background in a systemic, untargeted manner, the present *in vitro* approach is exploring metabolic change in macrophages upon specific cytokine stimulation, which represents a more targeted and complementary approach. We are describing a highly efficient and reproducible read out system for characterizing the gross metabolic background of all metabolically relevant compartments involved (i.e., macrophage, parasite and growth media) via ^{1}H NMR spectroscopy. The well-defined compartmentalization and the known baseline metabolic compositions allow much clearer conclusion toward biomarker origin and metabolic translocation across the compartments, compared to complex mammalian systems. The approach therefore holds promise to offer substantial support in identifying parasite-derived compounds as candidate diagnostic biomarkers. Moreover, the efficiency of the presented testing system may be further exploited for evaluating potential parasiticidal metabolic supplements, novel drug candidates, and varying cytokine stimuli and can be easily adaptable to other metabolic profiling platforms if need be. We believe that integration of this more focused *in vitro* strategy into the landscape of untargeted metabolic profiling will help us to access the wealth of information waiting to be explored within the immune-metabolic interface.

AUTHOR INFORMATION

Corresponding Author

*Tel.: +44 20 7594-3899. E-mail: jasmina.saric@imperial.ac.uk. Tel.: +44 20 7594-3732. E-mail: i.muller@imperial.ac.uk.

Notes

The authors declare no competing financial interest.

ACKNOWLEDGMENTS

We thank the Wellcome Trust for financial support of the research presented in the current manuscript (Sir Henry Wellcome Fellowship JS, Award number P23665) and the MRC and The Faculty of Medicine at Imperial College for the MRC studentship which provided additional funds for SL. We would also like to acknowledge Dr. Kirill Veselkov for offering updated data processing scripts and general statistical advice.

REFERENCES

(1) WHO *The world health report 2004*; WHO, 2004.
(2) McConville, M. J.; de Souza, D.; Saunders, E.; Likic, V. A.; Naderer, T. Living in a phagolysosome; metabolism of *Leishmania* amastigotes. *Trends Parasitol.* **2007**, *23* (8), 368.
(3) Oliveira, F.; Jochim, R. C.; Valenzuela, J. G.; Kamhawi, S. Sand flies, *Leishmania*, and transcriptome-borne solutions. *Parasitol. Int.* **2009**, *58* (1), 1.
(4) Reithinger, R.; Dujardin, J. C.; Louzir, H.; Pirmez, C.; Alexander, B.; Brooker, S. Cutaneous leishmaniasis. *Lancet Infect. Dis.* **2007**, *7* (9), 581.
(5) Dedet, J. P. P., F. In *Manson's tropical diseases*; Cook, G. C. Z., A. I., Ed. 2009.
(6) Rosenthal, E.; Marty, P.; del Giudice, P.; Pradier, C.; Ceppi, C.; Gastaut, J. A.; Le Fichoux, Y.; Cassuto, J. P. HIV and *Leishmania* coinfection: a review of 91 cases with focus on atypical locations of Leishmania. *Clin. Infect. Dis.* **2000**, *31* (4), 1093.
(7) Beil, W. J.; Meinardus-Hager, G.; Neugebauer, D. C.; Sorg, C. Differences in the onset of the inflammatory response to cutaneous leishmaniasis in resistant and susceptible mice. *J. Leukoc. Biol.* **1992**, *52* (2), 135.
(8) Louis, J.; Moedder, E.; Behin, R.; Engers, H. Recognition of protozoan parasite antigens by murine T lymphocytes. I. Induction of specific T lymphocyte-dependent proliferative response to *Leishmania tropica*. *Eur. J. Immunol.* **1979**, *9* (11), 841.
(9) Mitchell, G. F.; Curtis, J. M.; Scollay, R. G.; Handman, E. Resistance and abrogation of resistance to cutaneous leishmaniasis in reconstituted BALB/c nude mice. *Aust. J. Exp. Biol. Med. Sci.* **1981**, *59* (Pt 5), 539.
(10) Howard, J. G.; Hale, C.; Chan-Liew, W. L. Immunological regulation of experimental cutaneous leishmaniasis. 1. Immunogenetic aspects of susceptibility to *Leishmania tropica* in mice. *Parasite Immunol.* **1980**, *2* (4), 303.
(11) Mosmann, T. R.; Coffman, R. L. TH1 and TH2 cells: different patterns of lymphokine secretion lead to different functional properties. *Annu. Rev. Immunol.* **1989**, 7145.
(12) Tato, C. M.; Laurence, A.; O'Shea, J. J. Helper T cell differentiation enters a new era: le roi est mort; vive le roi! *J. Exp. Med.* **2006**, *203* (4), 809.
(13) O'Shea, J. J.; Paul, W. E. Mechanisms underlying lineage commitment and plasticity of helper CD4+ T cells. *Science* **2010**, *327* (5969), 1098.
(14) Murphy, K. M.; Stockinger, B. Effector T cell plasticity: flexibility in the face of changing circumstances. *Nat. Immunol.* **2010**, *11* (8), 674.
(15) Noel, W.; Raes, G.; Hassanzadeh Ghassabeh, G.; De Baetselier, P.; Beschin, A. Alternatively activated macrophages during parasite infections. *Trends Parasitol.* **2004**, *20* (3), 126.
(16) Kropf, P.; Fuentes, J. M.; Fahnrich, E.; Arpa, L.; Herath, S.; Weber, V.; Soler, G.; Celada, A.; Modolell, M.; Muller, I. Arginase and polyamine synthesis are key factors in the regulation of experimental leishmaniasis *in vivo*. *FASEB J.* **2005**, *19* (8), 1000.
(17) Alberati-Giani, D.; Malherbe, P.; Ricciardi-Castagnoli, P.; Kohler, C.; Denis-Donini, S.; Cesura, A. M. Differential regulation of indoleamine 2,3-dioxygenase expression by nitric oxide and inflammatory mediators in IFN-gamma-activated murine macrophages and microglial cells. *J. Immunol.* **1997**, *159* (1), 419.
(18) Li, P.; Yin, Y. L.; Li, D.; Kim, S. W.; Wu, G. Amino acids and immune function. *Br. J. Nutr.* **2007**, *98* (2), 237.
(19) Wu, G.; Meininger, C. J. Regulation of nitric oxide synthesis by dietary factors. *Annu. Rev. Nutr.* **2002**, 2261.
(20) Choi, B. S.; Martinez-Falero, I. C.; Corset, C.; Munder, M.; Modolell, M.; Muller, I.; Kropf, P. Differential impact of L-arginine

deprivation on the activation and effector functions of T cells and macrophages. *J. Leukoc. Biol.* **2009**, *85* (2), 268.
(21) Kropf, P.; Baud, D.; Marshall, S. E.; Munder, M.; Mosley, A.; Fuentes, J. M.; Bangham, C. R.; Taylor, G. P.; Herath, S.; Choi, B. S.; Soler, G.; Teoh, T.; Modolell, M.; Muller, I. Arginase activity mediates reversible T cell hyporesponsiveness in human pregnancy. *Eur. J. Immunol.* **2007**, *37* (4), 935.
(22) Modolell, M.; Choi, B. S.; Ryan, R. O.; Hancock, M.; Titus, R. G.; Abebe, T.; Hailu, A.; Muller, I.; Rogers, M. E.; Bangham, C. R.; Munder, M.; Kropf, P. Local suppression of T cell responses by arginase-induced L-arginine depletion in nonhealing leishmaniasis. *PLoS Negl. Trop. Dis.* **2009**, *3* (7), e480.
(23) Saric, J.; Li, J. V.; Wang, Y.; Keiser, J.; Veselkov, K.; Dirnhofer, S.; Yap, I. K.; Nicholson, J. K.; Holmes, E.; Utzinger, J. Panorganismal metabolic response modeling of an experimental *Echinostoma caproni* infection in the mouse. *J. Proteome Res.* **2009**, *8* (8), 3899.
(24) Wang, Y.; Utzinger, J.; Saric, J.; Li, J. V.; Burckhardt, J.; Dirnhofer, S.; Nicholson, J. K.; Singer, B. H.; Brun, R.; Holmes, E. Global metabolic responses of mice to *Trypanosoma brucei brucei* infection. *Proc. Natl. Acad. Sci. U.S.A.* **2008**, *105* (16), 6127.
(25) Saric, J.; Li, J. V.; Swann, J. R.; Utzinger, J.; Calvert, G.; Nicholson, J. K.; Dirnhofer, S.; Dallman, M. J.; Bictash, M.; Holmes, E. Integrated cytokine and metabolic analysis of pathological responses to parasite exposure in rodents. *J. Proteome Res.* **2010**, *9* (5), 2255.
(26) Saric, J.; Li, J. V.; Utzinger, J.; Wang, Y.; Keiser, J.; Dirnhofer, S.; Beckonert, O.; Sharabiani, M. T.; Fonville, J. M.; Nicholson, J. K.; Holmes, E. Systems parasitology: effects of *Fasciola hepatica* on the neurochemical profile in the rat brain. *Mol. Syst. Biol.* **2010**, 6396.
(27) Birungi, G.; Chen, S. M.; Loy, B. P.; Ng, M. L.; Li, S. F. Metabolomics approach for investigation of effects of dengue virus infection using the EA.hy926 cell line. *J. Proteome Res.* **2010**, *9* (12), 6523.
(28) Ellis, J. K.; Chan, P. H.; Doktorova, T.; Athersuch, T. J.; Cavill, R.; Vanhaecke, T.; Rogiers, V.; Vinken, M.; Nicholson, J. K.; T, M. D. E.; Keun, H. C. Effect of the histone deacetylase inhibitor trichostatin a on the metabolome of cultured primary hepatocytes. *J. Proteome Res.* **2010**, *9* (1), 413.
(29) Ellis, J. K.; Athersuch, T. J.; Cavill, R.; Radford, R.; Slattery, C.; Jennings, P.; McMorrow, T.; Ryan, M. P.; Ebbels, T. M.; Keun, H. C. Metabolic response to low-level toxicant exposure in a novel renal tubule epithelial cell system. *Mol. Biosyst.* **2011**, *7* (1), 247.
(30) Beckonert, O.; Coen, M.; Keun, H. C.; Wang, Y.; Ebbels, T. M.; Holmes, E.; Lindon, J. C.; Nicholson, J. K. High-resolution magic-angle-spinning NMR spectroscopy for metabolic profiling of intact tissues. *Nat. Protoc.* **2010**, *5* (6), 1019.
(31) Meiboom, S. G. D. Modified spin-echo method for measuring nuclear relaxation times. *Rev. Sci. Instrum.* **1958**, 29688.
(32) Cloarec, O.; Dumas, M. E.; Craig, A.; Barton, R. H.; Trygg, J.; Hudson, J.; Blancher, C.; Gauguier, D.; Lindon, J. C.; Holmes, E.; Nicholson, J. Statistical total correlation spectroscopy: an exploratory approach for latent biomarker identification from metabolic ^{1}H NMR data sets. *Anal. Chem.* **2005**, *77* (5), 1282.
(33) Veselkov, K. A.; Vingara, L. K.; Masson, P.; Robinette, S. L.; Want, E.; Li, J. V.; Barton, R. H.; Boursier-Neyret, C.; Walther, B.; Ebbels, T. M.; Pelczer, I.; Holmes, E.; Lindon, J. C.; Nicholson, J. K. Optimized preprocessing of ultra-performance liquid chromatography/mass spectrometry urinary metabolic profiles for improved information recovery. *Anal. Chem.* **2011**, *83* (15), 5864.
(34) Dieterle, F.; Ross, A.; Schlotterbeck, G.; Senn, H. Probabilistic quotient normalization as robust method to account for dilution of complex biological mixtures. Application in ^{1}H NMR metabonomics. *Anal. Chem.* **2006**, *78* (13), 4281.
(35) Eriksson, L.; Antti, H.; Gottfries, J.; Holmes, E.; Johansson, E.; Lindgren, F.; Long, I.; Lundstedt, T.; Trygg, J.; Wold, S. Using chemometrics for navigating in the large data sets of genomics, proteomics, and metabonomics (gpm). *Anal. Bioanal. Chem.* **2004**, *380* (3), 419.
(36) Trygg, J.; Holmes, E.; Lundstedt, T. Chemometrics in metabonomics. *J. Proteome Res.* **2007**, *6* (2), 469.
(37) Cloarec, O.; Dumas, M. E.; Trygg, J.; Craig, A.; Barton, R. H.; Lindon, J. C.; Nicholson, J. K.; Holmes, E. Evaluation of the orthogonal projection on latent structure model limitations caused by chemical shift variability and improved visualization of biomarker changes in ^{1}H NMR spectroscopic metabonomic studies. *Anal. Chem.* **2005**, *77* (2), 517.
(38) Trygg, J. W. S. Orthogonal projections to latent structures (O-PLS). *J. Chemom.* **2002**, *16* (3), 119.
(39) Munder, M.; Eichmann, K.; Modolell, M. Alternative metabolic states in murine macrophages reflected by the nitric oxide synthase/arginase balance: competitive regulation by CD4+ T cells correlates with Th1/Th2 phenotype. *J. Immunol.* **1998**, *160* (11), 5347.
(40) Opperdoes, F. R.; Coombs, G. H. Metabolism of Leishmania: proven and predicted. *Trends Parasitol.* **2007**, *23* (4), 149.
(41) Li, Z.; Vance, D. E. Phosphatidylcholine and choline homeostasis. *J. Lipid Res.* **2008**, *49* (6), 1187.
(42) Wyss, M.; Kaddurah-Daouk, R. Creatine and creatinine metabolism. *Physiol. Rev.* **2000**, *80* (3), 1107.
(43) Naderer, T.; McConville, M. J. The *Leishmania*-macrophage interaction: a metabolic perspective. *Cell Microbiol.* **2008**, *10* (2), 301.
(44) Garedew, A.; Henderson, S. O.; Moncada, S. Activated macrophages utilize glycolytic ATP to maintain mitochondrial membrane potential and prevent apoptotic cell death. *Cell Death Differ.* **2010**, *17* (10), 1540.
(45) Zeisel, S. H.; Mar, M. H.; Howe, J. C.; Holden, J. M. Concentrations of choline-containing compounds and betaine in common foods. *J. Nutr.* **2003**, *133* (5), 1302.